BBA - Molecular Basis of Disease 1865 (2019) 2618–2632

Contents lists available at ScienceDirect

BBA - Molecular Basis of Disease

journal homepage: www.elsevier.com/locate/bbadis

Directed elimination of senescent cells attenuates development of osteoarthritis by inhibition of c-IAP and XIAP

Wang Peilin[a,b,1,2], Teng Songsong[a,1,2], Zhuang Chengyu[c,1,3], Cui Zhi[a,b,2], Ma Chunhui[a,2], Yu Yinxian[a,2], Zhou Lei[a,b,2], Mao Min[a,b,4], Wang Zongyi[a,b,4], Yang Mengkai[a,b,4], Xu Jing[a,b,4], Zhang Tao[a,b,4], Wang Zhuoying[a,b,4], Yin Fei[a,b,4], Yi Chengqing[a,*]

[a] Department of Orthopaedics, Shanghai General Hospital, Shanghai Jiao Tong University School of Medicine, Shanghai, China
[b] Shanghai Bone Tumor Institute, Shanghai, China
[c] Department of Orthopaedics, Rui Jin Hospital, Shanghai Jiao Tong University School of Medicine, Shanghai, China

ARTICLE INFO

Keywords:
Senescence
IAPs
AT-406
Osteoarthritis
Apoptosis
Autophagy

ABSTRACT

Aging drives the accumulation of senescent cells (SnCs) by secreting factors that cause the senescence-associated secretory phenotype (SASP), including stem cells in the bone marrow, which contribute to aging-related bone degradation. Osteoarthritis (OA) is a serious chronic injury disease, and increasing age is a major risk factor. The accumulation of SnCs may accelerate the development of OA, and the accumulation of SnCs may benefit from its resistance to apoptotic stimuli. Therefore, local elimination of SnCs could be a promising treatment for OA. Apoptosis inhibitor protein (IAP) is an important antiapoptotic protein in vivo. AT-406 is a small molecule inhibitor of the IAP genes and also regulates the transcription of several genes. Here, we show that SnCs up-regulate the antiapoptotic proteins c-IAP1, c-IAP2 and XIAP.The combined inhibition of c-IAP1, c-IAP2 and XIAP using siRNA or AT-406 specifically induce the apoptosis of SnCs.In addition, XIAP and STX17 bind to each other to regulate the fusion of autophagosomes and lysosomes in SnCs, which in turn, affects the fate of SnCs. It is worth noting that the clearance of SnCs attenuated the secretion of SASP and created a proregenerative environment. Most importantly, local clearance of SnCs significantly attenuated the progression of osteoarthritis in rats without significant toxic effects. Thus, local elimination of SnCs may be a potential treatment for OA. This is the first report of inhibition of IAPs for clearing SnCs and suggests that eradication of SnCs may be a new strategy for the treatment of age-related diseases.

1. Introduction

Cellular senescence is a stable state of cell cycle arrest, and proliferation potential can be limited by a variety of cell responses to stress [1]. Although cellular senescence is one of the mechanisms that can prevent premalignant lesions from continuing to worsen, the long-standing presence of senescent cells in tissues appears to be detrimental [2]. Senescent cells accumulate in many vertebrate tissues with age, and these tissues may lead to the secretion of senescence-associated secretory phenotype (SASP) factors, leading to age-related diseases [3].

Osteoarthritis (OA) is a chronic degenerative disease characterized by pain and activity disorders that are caused by degeneration of articular cartilage, which prevalence was increases with age [4]. More importantly, very similar characteristics of inflammation and catabolic media were observed during the pathogenesis of OA and “classic” senescent cells. [5]. As a seed cell for tissue engineering, bone marrow mesenchymal stem cells (BMSCs) have osteogenic and chondrogenic differentiation potential and play important roles in bone metabolism and bone tissue repair. During OA, various aging markers in BMSCs performed more prominently, such as cell cycle arrest, SASP secretion, and reduced differentiation [6]. Therefore, senescent cells in tissues may play a pathological role in the etiology of OA. It has been reported

* Corresponding author at: 100 Haining Road Shanghai, Shanghai General Hospital, Shanghai Jiao Tong University School of Medicine, Shanghai, China.
E-mail addresses: wzy1992@sjtu.edu.cn (W. Zongyi), zhangtaoabc@2008.sina.com (Z. Tao), chengqing.yi@shgh.cn (Y. Chengqing).
[1] These authors contributed equally to this work.
[2] Department of Orthopaedics, 100 Haining Road Shanghai, Shanghai General Hospital, Shanghai Jiao Tong University School of Medicine, Shanghai, China.
[3] Department of Orthopaedics, 197 Ruijin Road II Shanghai, Rui Jin Hospital, Shanghai Jiao Tong University School of Medicine, Shanghai, China.
[4] Department of Orthopaedics, Shanghai Bone Tumor Institute, 100 Haining Road Shanghai, Shanghai General Hospital, Shanghai Jiao Tong University School of Medicine, Shanghai, China.

https://doi.org/10.1016/j.bbadis.2019.05.017
Received 11 December 2018; Received in revised form 28 April 2019; Accepted 27 May 2019
Available online 26 June 2019

that injecting senescent cells into normal mice can cause aging of organs in mice and various physiological dysfunctions [7]. The clearance of senescent cells in a premature aging mouse was shown restoration of physiological function and reduction of tissue aging [8]. Therefore, the removal of senescent cells may effectively delay the progression of age-related diseases and prolong healthy life [9].

It is reported that senescent cells are resistant to exogenous and endogenous pro-apoptotic stimuli [10]. Although the mechanisms that drive aging have been well studied, an understanding of the mechanisms that confer increased survivability of these cells is limited [11]. IAP genes play a central role in the regulation of cell death through a variety of mechanisms, including apoptosis and autophagy [12]. The IAP family of genes includes antiapoptotic proteins c-IAP1, c-IAP2, XIAP, BRUCE, Livin and Survivin, etc., which have been intensively studied as targets for cancer drug intervention [13]. We evaluated the individual contributions of these IAP family members to senescence cell viability, and we studied the mechanisms by which the expression of key members, c-IAP1, c-IAP2 and XIAP, is increased in senescent cells to inhibit apoptosis. We show that the inhibitors targeting c-IAP1, c-IAP2 and XIAP proteins (AT-406) preferentially clear senescent cells in vitro and in vivo and restore the differentiation ability of BMSCs to delay the progression of OA. Collectively, these findings support the use of SnCs as a therapeutic target for the treatment of OA.

2. Results

2.1. The proteins of IAP family upregulated in senescent cells

To examine resistance to apoptotic pathways in senescent cells, we induced mesenchymal stem cell (MSC) aging by three different methods: treatment with a suitable concentration of D-gal (DS); treatment with a suitable concentration of H_2O_2 (HS); and replicative exhaustion for replicative senescence (RS). We treated MSCs with different doses of D-gal and H_2O_2 at various time points and measured cell viability via a CCK8 assay. We found that cell viability was inhibited by D-gal and H_2O_2 in a time- and dose-dependent manner. According to the IC_{50} value and the obvious downward trend (Supplementary Fig. 1A and B), induction by 10 g/LL D-gal and 100 mM H_2O_2 for 48 h was used in the subsequent experiments. For replication failure, we chose seventh generation cells as the RS group. To confirm whether the cells in the three different treatment states were senescent cells, we evaluated the cell cycle state and the apoptosis state of the three groups of cells. The results showed that the G0-G1 phase of the three groups of cells were blocked to different degrees (DS: 64.2%, HS: 57.8%, RS: 61.4%, Supplementary Fig. 1C) and almost no apoptosis was observed (DS: 5.1%, HS: 6.3%, RS: 3.9%, Supplementary Fig. 1D) compared with the control group. Then, we performed SA-b-gal staining and found that the aging group had a significantly increased proportion of SA-b-gal-positive cells compared with the control group (DS: 65.7%, HS: 71.3%, RS: 58.6%, Supplementary Fig. 1E). We detected the level of gammaH2AX as markers of DNA damage levels by immunofluorescence in the three groups of senescent cells (Supplementary Fig. 1F). The results showed that the damaged DNA was accumulated in the nucleus of senescent cells, compared with the control group.

After determining that the three groups of treated cells were in an aging state, senescent and control MSCs were treated with tumor necrosis factor-α (TNF-α) and cycloheximide (CHX) to induce the apoptotic pathway. After TNF-α treatment, the survival rate of the three groups of aging cells was significantly higher than that of the control group (68.9%, 66.7% or 71.2% versus 38.9% for DS, HS or RS cells versus growing cells (G); Fig. 1A). The reduction of cleavage of the three markers to confirm a decrease in apoptosis in senescent cells, including: poly-ADP-ribose polymerase (PARP), caspase-9 and caspase-3 (Fig. 1B). Finally, we have determined the direct effects of TNF-< alpha > and CHX on the level of c-IAP1, c-IAP2 and XIAP. The results showed that there was no significant difference in the expression level of c-IAP1, c-IAP2 and XIAP after the treatment of TNF-α, and CHX could reduce their expression levels (Supplementary Fig. 2A). These findings confirm that senescent cells are more resistant to pro-apoptotic stimuli compare with non-senescent cells.

We hypothesized that an increase in the level of anti-apoptotic proteins is responsible for the resistance of senescent cells to apoptosis. The inhibitor of apoptosis (IAP) is a widely known anti-apoptotic protein with highly conserved properties [14]. We tested the levels of the anti-apoptotic proteins c-IAP1, c-IAP2 and XIAP in senescent and control (G) cells. The expression levels of c-IAP1, c-IAP2 and XIAP were increased in the senescent MSCs of the three different treatment groups (Fig. 1C). Subsequently, we performed immunofluorescence (Fig. 1D) and qPCR (Supplementary Fig. 2B) analyses of the three IAP family members to further explain the above conclusions.

In light of the consistent upregulation of c-IAP1, c-IAP2 and XIAP observed in senescent cells of all tested types, we used AT-406, a potent small-molecule inhibitor of c-IAP1, c-IAP2 and XIAP, to inhibit these genes and observe the effects on cell viability, as shown in Supplementary Fig. 2C. All three types of senescent cells were significantly more sensitive to AT-406 treatment than control cells (Fig. 1E). We then verified that AT-406 inhibits the expression of c-IAP1, c-IAP2 and XIAP at the IC_{50} concentration (Fig. 1F). In order to determine if AT-406-treated senescent cells experienced apoptosis, the AT-406 treatment of senescent cells with or without the pan-caspase inhibitor z-VAD-fmk (Fig. 1G). This inhibitor almost completely prevented the reduction of senescent cells viability by AT-406 and eliminated the increased cleavage of PARP, caspase-9 and caspase-3 in senescent cells (Fig. 1H). We obtained the same result using flow cytometry (Supplementary Fig. 2D). These findings indicate that these IAP family genes confer resistance of senescent cells to apoptosis and promote senescent cell survival.

2.2. cIAP1, cIAP2 and XIAP maintain the viability of senescent cells

To determine whether extensive inhibition of IAP family members by different inhibitors also resulted in reduced viability of senescent cells, we treated BMSCs with AZD5582, an inhibitor of c-IAP1, c-IAP2 and XIAP. Similarly, AZD5582 caused significantly higher death rates in aging cells than in control cells (62% of remaining adherent growing cells versus 31% of DS cells; versus 26% of HS cells; and versus 39% of RS cells; Fig. 2A). Therefore, death of senescent cells can be specifically induced by AZD5582. Next, we investigated the individual contributions of cIAP1, cIAP2 and XIAP to the resistance of senescent cells to apoptosis. No specific inhibitor can inhibit only one of the three, but c-IAP1 and XIAP can be specifically inhibited by BV6. Interestingly, despite a dose-dependent decrease in cell viability after senescent cells were treated with BV6, the degree of reduction was far less significant than the response to AZD5582 treatment (Fig. 2B).

To further investigate the contribution of c-IAP1, c-IAP2 and XIAP to senescence-resistant apoptosis in senescent cells, we used siRNA to silence the three genes individually or together. Combinational silencing of the three genes effectively reduced their protein levels, but silencing these genes, alone or in combination, resulted in a slight decrease in aging cell viability in the DS group (Fig. 2C&D). In contrast, the combined knockdown of c-IAP1, c-IAP2 and XIAP had a synergistic effect, resulting in a significant decrease in DS cell viability (42%) comparable to that induced by AT-406 treatment (Fig. 2D). These results suggest that at least one of c-IAP1, c-IAP2 and XIAP may be required for senescent cell survival.

2.3. Regulation of the expression of IAP genes and increased apoptosis resistance in senescent cells

After determining the contribution of the IAP genes to aging cell apoptosis resistance, we next investigated the causes of elevated IAP genes in senescent cells and the reasons for their inhibition of apoptosis.

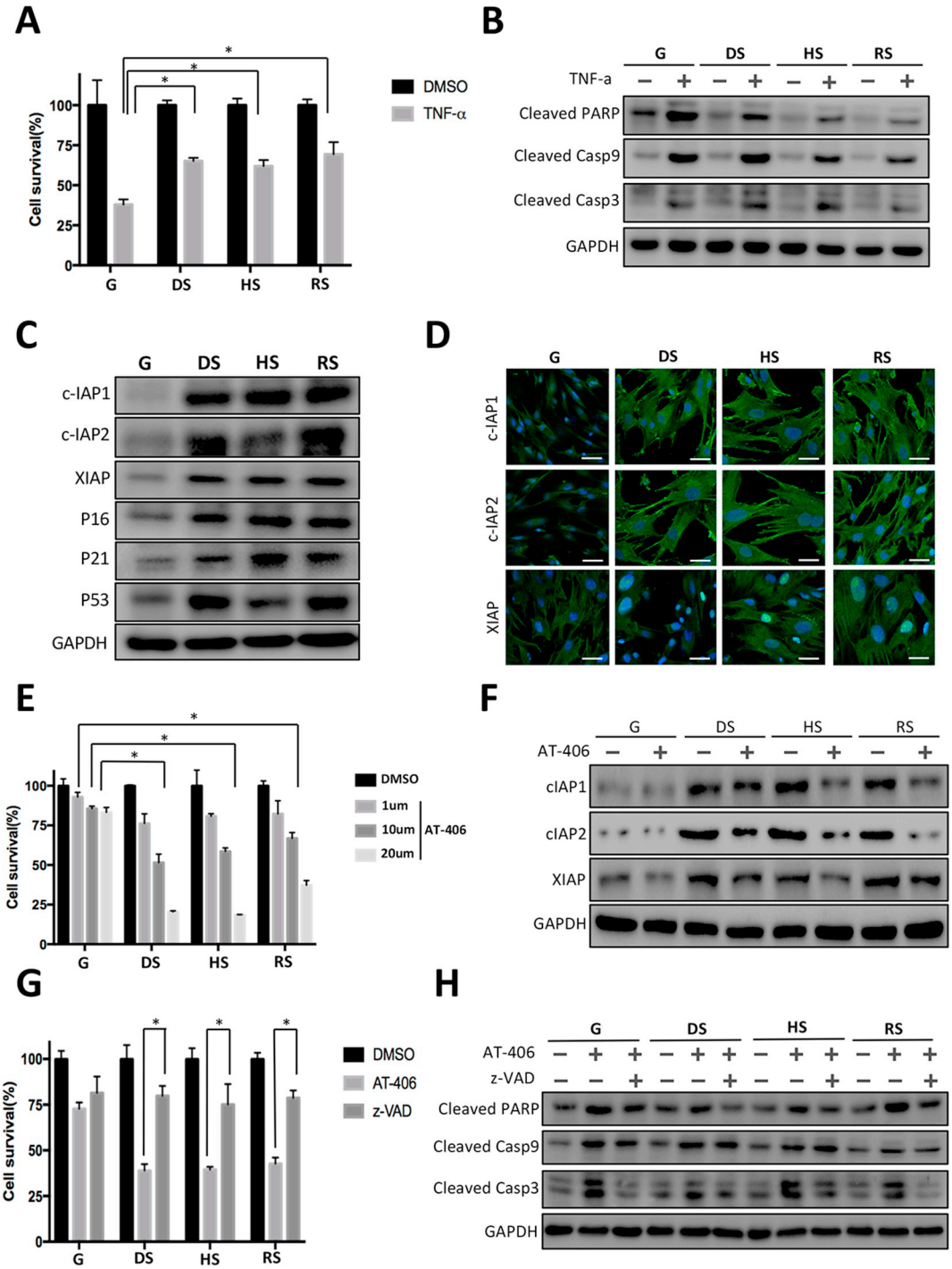

Fig. 1. The proteins of IAP family upregulated in senescent cells and provide resistance to apoptosis. (A) Rat BMSCs that were induced to senescence either through D-gal induction (DS), H_2O_2 induction (HS) or replicative exhaustion (RS) and control proliferating cells (growing, G) were treated with TNF-α (TNF-α) or vehicle (DMSO) for 10 h. Determination of survival relative to vehicle-treated cells by quantifying remaining adherent cells. The histograms represent the percentage of senescent (DS, HS, and RS) cells that survived compared to the G controls. (B) The cleavage of PARP, caspase-9 and caspase-3 protein expression by senescent cells and control cells was analyzed by Western blot, indicating the level of apoptosis after treatment with TNF-α and CHX. (C) Western blot analysis of IAP family members (c-IAP1, c-IAP2 and XIAP) and senescence effector proteins (p16, p21, p53) expression in senescence (DS, HS and RS) and control (G) BMSC. (D) Immunofluorescence staining showing c-IAP1, c-IAP2 and XIAP distributions in control cells and in the three groups of senescent cells; nuclei were stained by DAPI (blue). Scale bar = 50 μm. (E) Percent survival of senescent and control cells (as in A) after 48 h of treatment with the indicated concentrations of AT-406 (inhibitors of c-IAP1, c-IAP2 and XIAP). (F) Related proteins in the three groups of senescent cells with or without AT-406 treatment. The protein levels of c-IAP1, c-IAP2 and XIAP were analyzed by Western blot. (G) Percentage of senescence and control cells treated with AT-406 (10 μM) for 48 h with pan-caspase inhibitor z-VAD-fmk (100 μM), with or without pretreatment for 6 h. (H) Western blot analysis of cleaved PARP, caspase-9 and caspase-3 in the samples described in G. The results shown here are representative of three independent experiments. The histograms represented the mean ± SD of three independent experiments. $^{*}P < 0.05$, $^{**}P < 0.01$, $^{***}P < 0.001$.

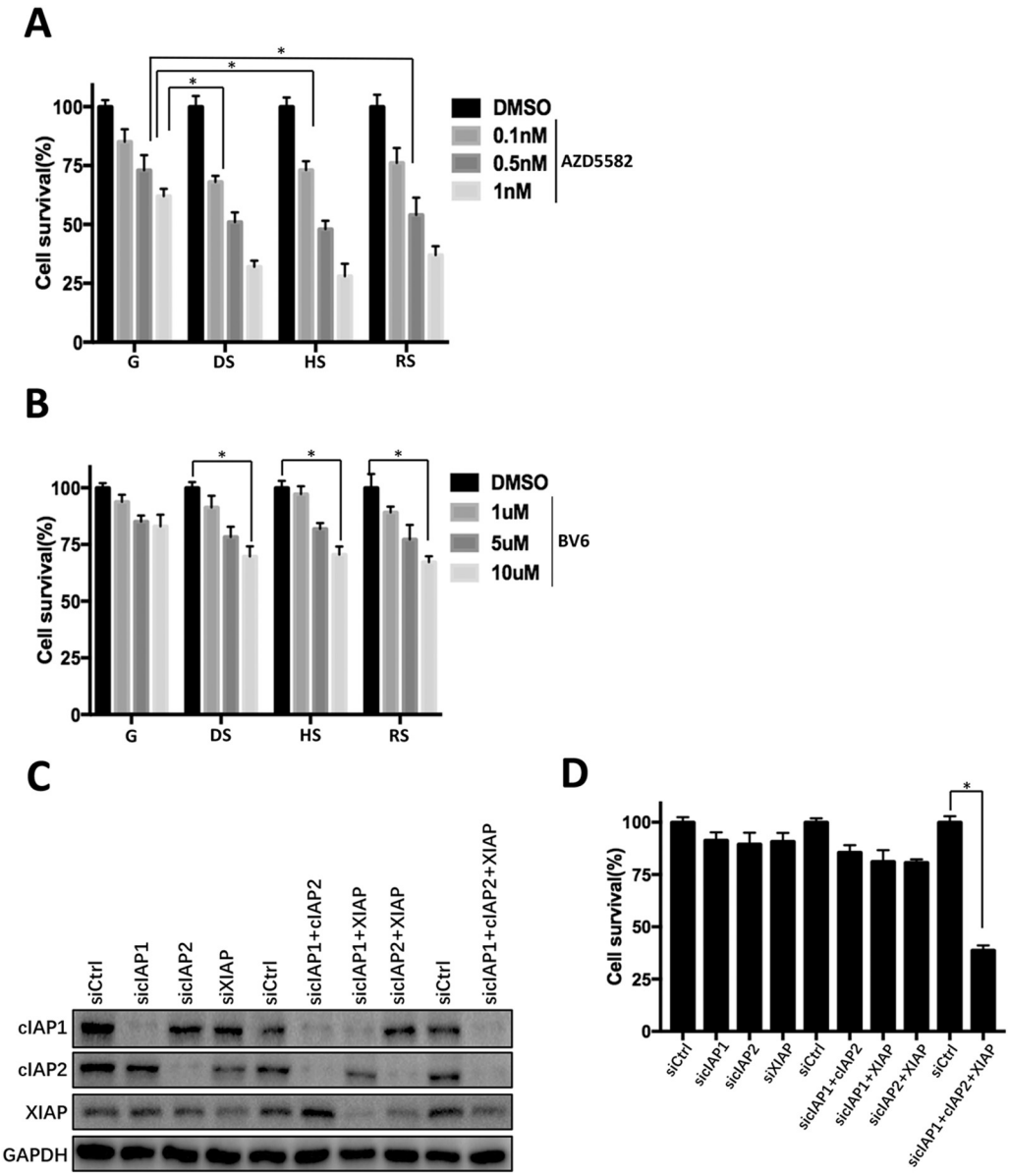

Fig. 2. cIAP1, cIAP2 and XIAP maintain the viability of senescent cells. (A) Rat BMSCs (DS, HS and RS cells and control G cells) were treated with the indicated concentrations of AZD5582 or vehicle (DMSO) for 48 h. Determination of survival relative to vehicle-treated cells by quantifying remaining adherent cells. The histograms represent the percentage of senescent (DS, HS, and RS) cells that survived compared to the G controls. (B) The percentage survival of cells described in A treated with the indicated concentration of BV6 for the next 48 h. (C) Western blot analysis of c-IAP1, c-IAP2 and XIAP following siRNA treatment of the DS group. (D) Percent survival of DS group cells transduced with siRNA targeting c-IAP1, c-IAP2 and XIAP or a combination thereof. The results shown here are representative of three independent experiments. The histograms represented the mean ± SD of three independent experiments. *P < 0.05, **P < 0.01, ***P < 0.001.

In recent years, the NF-κB pathway has been confirmed to be closely related to cellular senescence [15]. Although it has been previously reported that IAPs are downstream of the NF-κB pathway, it is still unknown whether this relationship exists in senescent cells [16].

First, we examined activation of the NF-κB pathway in three groups of senescent cells. BMSCs were treated with D-gal and H_2O_2 for 6, 12, 24 and 48 h, and the 6th, 7th, 8th, 9th or 10th generation of BMSCs were used. The expression levels of p65, p-p65, p-IκBα and IκBα were detected using Western blot. The results showed that the ratio of p-p65 to p65 and p-IκBα to IκBα increased with time (Fig. 3A). Next, we performed immunofluorescence microscopy and nuclear-cytoplasmic extraction, and the results further support the nuclear translocation of p65 in senescent cells (Fig. 3B&C). To determine the effects of NF-κB pathway activation on c-IAP1, c-IAP2 and XIAP in senescent cells, senescent cells were treated with IMD-0354, an inhibitor of the NF-κB pathway, and the expression levels of c-IAP1, c-IAP2 and XIAP were assessed using Western blotting. As shown in Fig. 3D, the expression levels of c-IAP1, c-IAP2 and XIAP were reduced after IMD-0354 treatment. In contrast, we used the IAP inhibitor AT-406 to treat senescent cells for 6, 12, 24 and 48 h and evaluated the expression levels of p65, p-p65, p-IκBα and IκBα. The NF-κB pathway was also blocked by AT-406 (Supplementary Fig. 3A). Our results are consistent with previous reports: although NF-κB can induce the expression of IAPs, inhibition of IAP can attenuate NF-κB signaling [14,17–19].

Next, we confirmed in greater detail that inhibition of the IAP gene can induce apoptosis of senescent cells. Three groups of senescent cells were treated with AT-406 for 6, 12, 24 and 48 h, and the expression levels of cleaved PARP, caspase-9 and caspase-3 were detected. As expected, the expression levels of cleaved PARP, caspase-9 and caspase-3 increased with AT-406 treatment time (Fig. 3E). Since it was previously reported that the IAP genes inhibit apoptosis through the MAPK signaling pathway, we detected whether the relationship between IAP genes and the MAPK signaling pathway still exists in senescent cells [20,21]. We treated three groups of senescent cells with AT-406 at 6, 12, 24 and 48 h and detected the expression levels of JNK, p-JNK, p38, p-p38, ERK, p-ERK and p-c-Jun. Western blot analysis showed that the ratio of p-JNK to JNK and the expression level of p-c-Jun increased with time, but the ratio of p-p38 to p38 and p-ERK to ERK did not change significantly (Fig. 3G). These results indicate that inhibition of IAPs activates the JNK pathway and promotes apoptosis in senescent cells.

The above findings illustrate that activation of the NF-κB pathway leads to increased expression of IAPs, which in turn inhibits the JNK

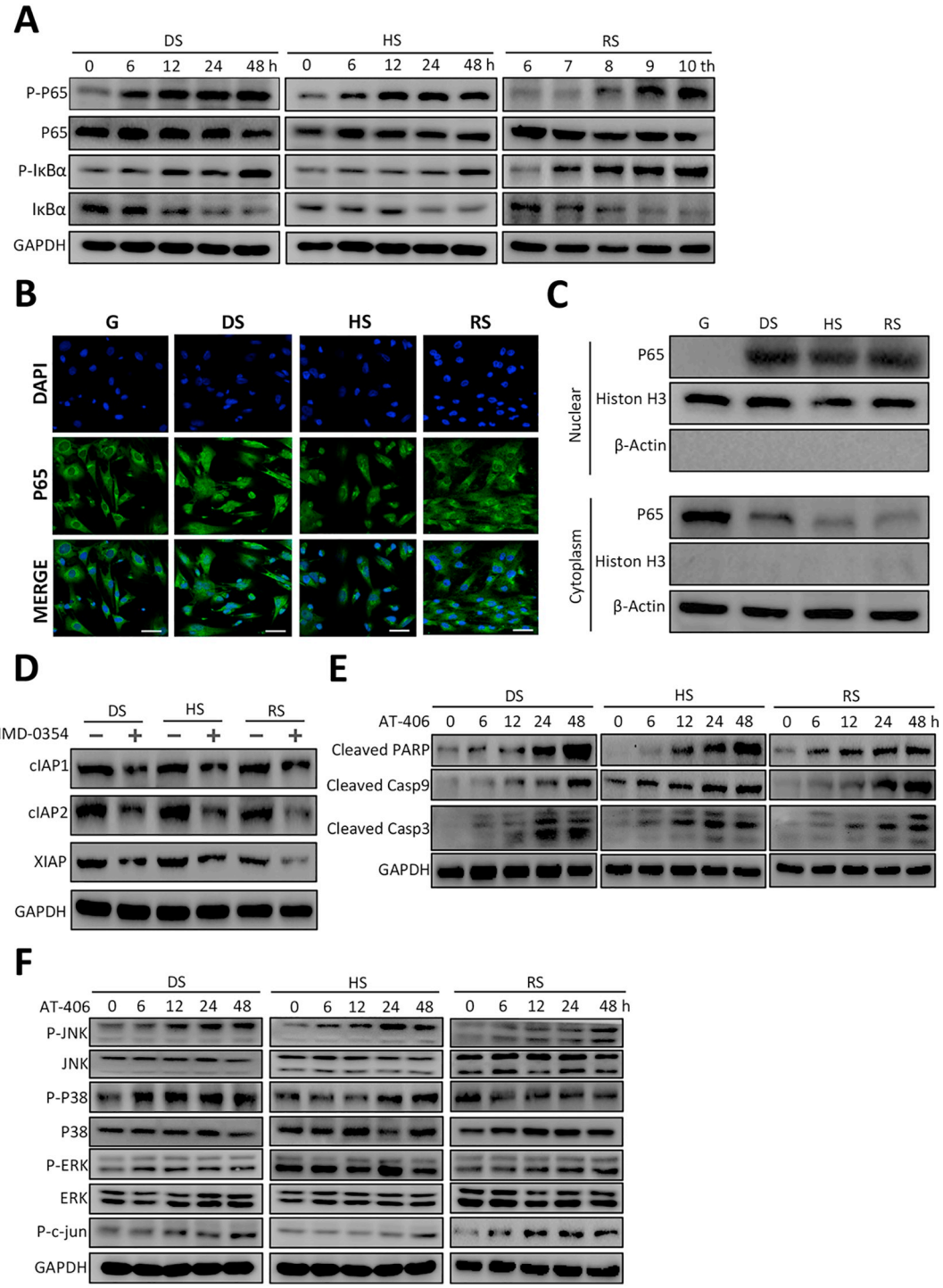

Fig. 3. IAP family members are elevated by activation of the NF-κB pathway and inhibit the JNK pathway to resist apoptosis in senescent cells. (A) The activity of NF-κB signaling pathways in rat BMSCs was detected by Western blot assays. (B) Immunofluorescence and nuclear-cytoplasmic extraction assays were used to determine the expression and nuclear translocation of NF-κB p65 in BMSCs. Scale bar = 50 μm. (C) The expression levels of P65 protein in the nucleus and cytoplasm were detected by Western blot assays. (D) Related proteins in the three groups of senescent cells with or without IMD-0354 treatment. The protein levels of c-IAP1, c-IAP2 and XIAP were analyzed by Western blot. (E) The expression levels of cleaved PARP, caspase-9 and caspase-3 in the samples were analyzed by Western blot. (F) MAPK signaling pathway activity in rat BMSCs was detected by Western blot assays. The results shown here are representative of three independent experiments.

pathway to confer apoptosis resistance.

2.4. XIAP regulates autophagosome–lysosome fusion in senescent cells

In our previous experiments, aging cell death was not completely inhibited after inhibition of the apoptotic pathway (Fig. 1G and Supplementary Fig. 2C). Therefore, cell fate could be influenced in other ways. In recent reports, it has been shown that the IAP family of genes are involved in autophagosome–lysosome fusion, and the imbalance of this process is often associated with cell death [22,23].

To validate our hypothesis, BMSCs were transiently transfected with GFP-mRFP-LC3B followed by treatment with D-gal or AT-406. In the tandem autophagosome reporter gene, GFP is pH sensitive and mRFP is resistant, so the GFP is quenched in the acidic environment of the

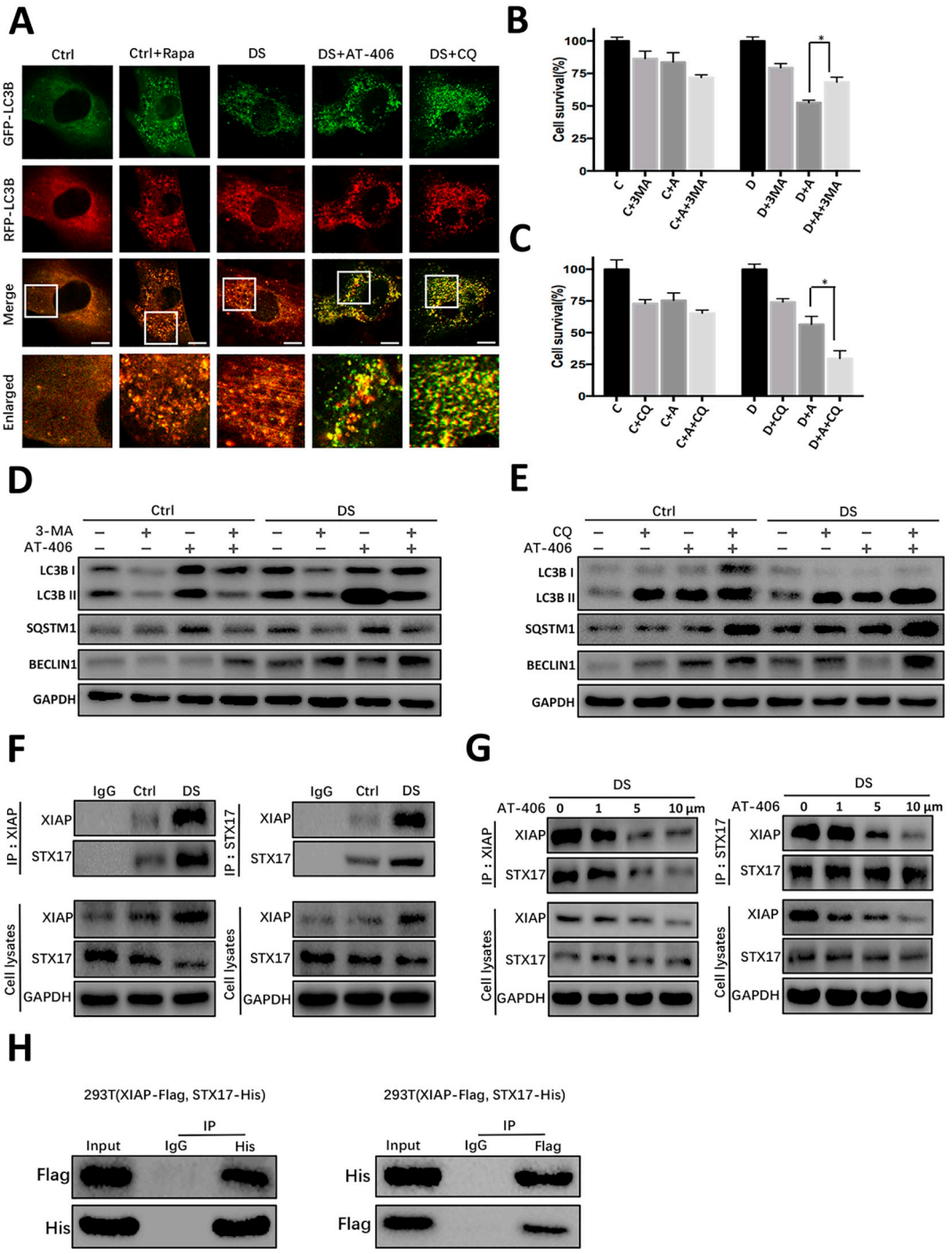

Fig. 4. XIAP interacts with STX17 to regulate the fusion of autophagosome–lysosomes in senescent cells. (A) Control cells, Rapa-treated control cells and AT-406 or CQ-treated DS group cells stably expressing GFP-mRFP-LC3B for confocal microscopy. Scale bar = 20 μm. (B) Transfected control or senescent cells treated with AT-406 alone, 3MA alone or AT-406/3MA in combination. (C) Transfected control or senescent cells treated with AT-406 alone, CQ alone or AT-406/CQ in combination. Cell viability in B&C was determined by quantifying the remaining adherent cells. (D) Western blot detected the expression levels of LC3B, SQSTM1 and BECLIN1 in the samples described in B. (E) Western blot detected the expression levels of LC3B, SQSTM1 and BECLIN1 in the samples described in C. (F) The cell lysate of the DS group cells was immunoprecipitated by anti-XIAP antibodies, anti-STX17 antibodies or the normal rabbit immunoglobulin G (IgG, as control antibodies). Western blotting was performed with anti-STX17 or anti-XIAP antibodies. (G) The DS group cells were treated with different concentrations of AT-406, followed by co-immunoprecipitation assays. (H) HEK293T cells were transfected with STX17-His and XIAP-Flag, and then immunoprecipitated using anti-His antibody, anti-Flag antibody or IgG. The immunoblotting was used to analyze the immunocomplexes. The results shown here are representative of three independent experiments. The histograms represented the mean ± SD of three independent experiments. $^{*}P < 0.05$, $^{**}P < 0.01$, $^{***}P < 0.001$.

lysosome [24]. Thus, the fusion of autophagosomes with lysosomes only shows red puncta and yellow puncta are missing. An autophagy inducer-rapamycin (Rapa) and an autophagy inhibitor-chloroquine (CQ) were added after transfection. As shown by the results, the majority of red spots indicated fusion of autophagosomes with lysosomes, whereas only a small fraction of the LC3B-positive puncta was yellow in rapamycin-treated cells. Conversely, most of the LC3B-positive spots were yellow due to blockade of the autophagy process in CQ-

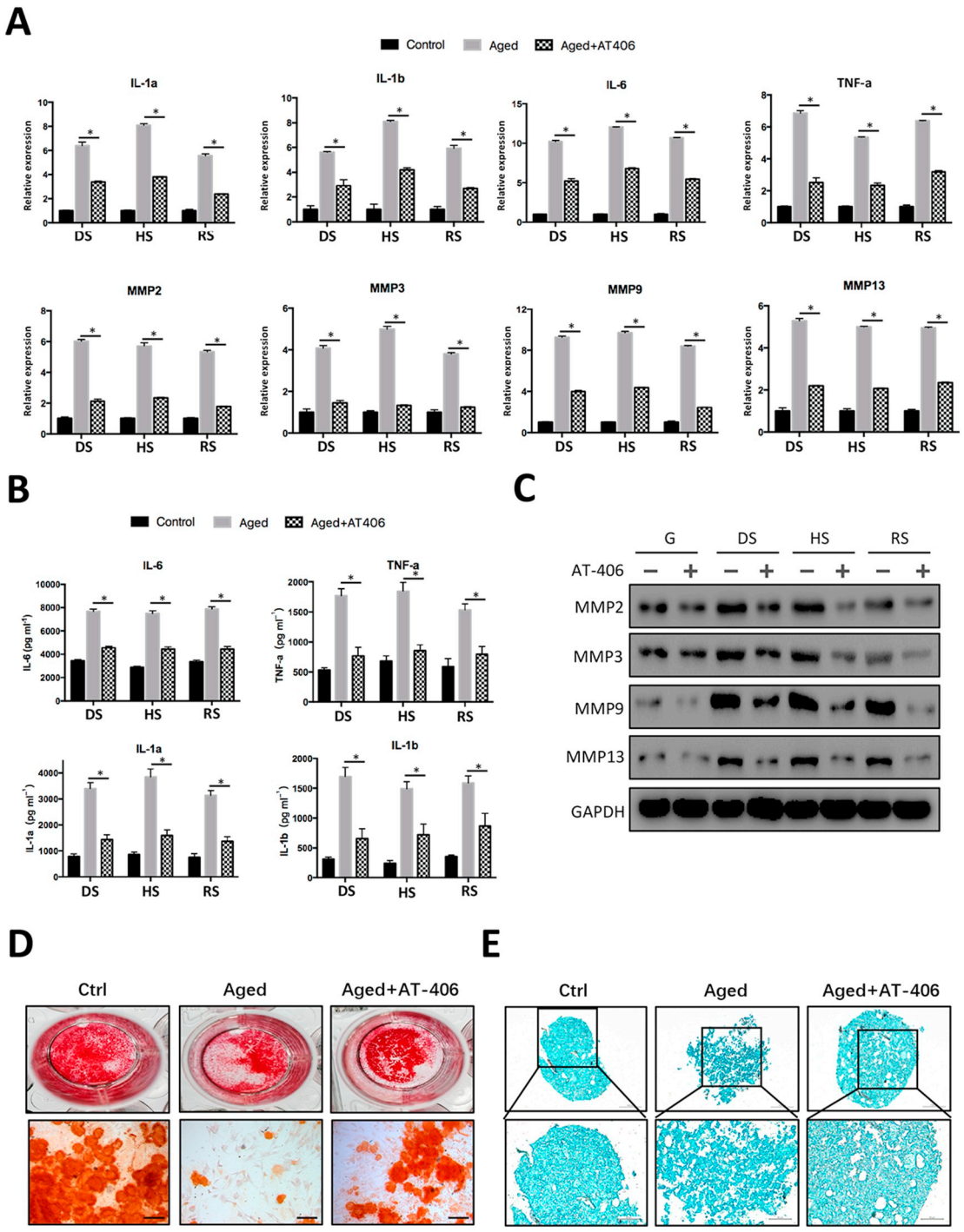

Fig. 5. Clearance of senescent cells reduces inflammatory factor secretion and creates a proregenerative environment. (A) The effect of AT-406 on the expression of MMP-2, -3, -9, -13, IL-1α, -1β, -6 and TNF-α genes in three groups of senescent cells were determined by qPCR. (B) The protein levels of IL-6, IL-1α, IL-1β and TNF-α in the supernatant were assessed by ELISA. (C) The expression levels of MMP-2, MMP-3, MMP-9 and MMP-13 were assessed by Western blot. (D) Alizarin red staining for osteogenic differentiation of BMSCs with or without conditioned medium treatment. Scale bar = 200 μm. (E) Alcian blue staining for chondrogenic differentiation of BMSCs with or without conditioned medium treatment. Scale bar = 100 μm. The histograms represented the mean ± SD of three independent experiments. *P < 0.05, **P < 0.01, ***P < 0.001.

treated cells. In the control group, LC3B diffused in the cytoplasm without aggregation, while in the DS group, LC3B-positive puncta aggregation also occurred, but fewer red spots were observed than in the rapamycin-treated group. This may be related to the induction of ROS production by D-gal treatment. In agreement with the results of the AT-406 treatment group, we found that the yellow spots increased and mixed with the red spots, but fewer yellow spots were observed than in the CQ treatment group (Fig. 4A). Similarly, we observed the same outcome in the HS group (Supplementary Fig. 4A). These phenomena suggest that inhibition of IAPs can block the fusion of autophagosomes with lysosomes.

Next, to determine whether blocking the process can increase the death of senescent cells, we used another autophagy inhibitor, 3-methyladenine (3MA), which can block the production of autophagic phagosomes. We treated the control and DS groups with 3MA or CQ in the presence or absence of AT-406 treatment, and we tested the survival

of cells in each treatment group. The results showed that the survival rate of senescent cells treated with AT-406 and 3MA was higher than that of cells treated with AT-406 in the DS group (68% versus 52%, Fig. 4B). In contrast, the survival rate of senescent cells treated with AT-406 and CQ was lower than that of cells treated with AT-406 in the DS group (29% versus 58%, Fig. 4C). As shown in Fig. 4C, in the presence of AT-406, the fusion of autophagosomes with lysosomes was blocked, causing excessive autophagy to damage cells, and thus, 3MA treatment can attenuate excessive autophagy to reduce senescent cell death. In contrast, CQ treatment can aggravate this phenomenon. We further tested the expression levels of LC3B, STSQM1 and BECLIN1 as markers of autophagy levels by Western blot in the above samples. The results showed that the LC3B-II and STSQM1 levels in the DS group were higher than those in the control group and increased with AT-406 treatment in both groups. However, after the addition of 3MA, the expression levels of LC3B-II and STSQM1 were reduced with or without AT-406 treatment in both groups. The expression of BECLIN1 followed the changes in LC3B-II expression (Fig. 4D). In contrast, after the addition of CQ, the expression levels of LC3B-II and STSQM1 further increased (Fig. 4E), indicating that the presence of AT-406 leads to the accumulation of autophagic phagosomes and autophagy-degrading substrates, which can be alleviated by the addition of 3MA. The above results indicate that inhibition of IAP genes can abolish the fusion of autophagosomes and lysosomes, causing death of senescent cells.

Subsequent experiments were performed to explore the mechanism of the IAP family of genes in regulating the fusion of autophagosomes with lysosomes. A previous study showed that STX17, an important member of the soluble N-ethylmaleimide-sensitive factor attachment protein receptor (SNARE), mediates the fusion of autophagosomes and lysosomes [25]. To test whether endogenous IAP genes interacts with stx17, coimmunoprecipitation experiments were performed using the control and DS groups. Indeed, endogenous XIAP and stx17 interact with each other (Fig. 4F). Similarly, we obtained the same results for the HS group (Supplementary Fig. 4B). Furthermore, coimmunoprecipitation experiments were performed using the DS groups treated with different concentrations of AT-406. The results showed that the expression of XIAP decreased with AT-406 treatment in a concentration-dependent manner, while AT-406 had no effect on the expression of STX17 (Fig. 4G). Furthermore, the interaction between exogenous XIAP and STX17 was demonstrated by coimmunoprecipitation assays in HEK293T cells (Fig. 4H). Therefore, AT-406 attenuates the interaction with STX17 by inhibiting the expression of XIAP, thereby inhibiting the fusion of autophagosomes with lysosomes.

2.5. IAP inhibition in senescent cells attenuates the secretion of SASP and creates a proregenerative environment

Given that inhibition of IAPs could clear senescent cells in our study, we further explored whether the elimination of senescent cells attenuated secretion of senescence-associated secretory phenotype (SASP) factors. Three groups of senescent cells were stimulated with AT-406 and detected the expression levels of inflammatory cytokines and catabolic genes, including TNF-α, interleukin(-1α, -1β, -6) and matrix metalloproteinase(-2, -3, -9, -13). Quantitative Real-time PCR showed that cellular senescence increased the transcription level of these genes, while pretreatment with AT-406 reversed this process by removing senescent cells (Fig. 5A). To further confirm the above results, we evaluated the effects of treatment with AT-406 on the secretion of IL-6, TNF-α, IL-1α and IL-1β in the supernatant by ELISA (Fig. 5B) and on the expression of MMP-2, MMP-3, MMP9 and MMP13 by Western blot (Fig. 5C).

Next, we explored whether the clearance of senescent cells could create a proregenerative environment. Conditioned medium (CM) was collected from senescent cell culture in the absence or presence of AT-406 over 48 h. The CM of senescent cells and the CM of senescent cells treated with AT-406 were added to normal cells, which were treated with osteogenic differentiation medium. The results showed that the osteogenic differentiation ability of cells treated with senescent CM was reduced compared with that of cells treated with normal CM and was increased after treatment with AT-406 CM (Fig. 5D). Similarly, we used CM to detect cartilage differentiation and got the same result (Fig. 5E).

2.6. AT-406 treatment rescues cartilage degeneration of post-traumatic osteoarthritis in rats in vivo

To explore whether the potential protective effects of articular cartilage in vivo by clearance of senescent cells, we first used H&E and Safranin O/Fast green staining to perform a histological analysis. Phosphate buffered saline (PBS)-treated ACLT rats exhibited a severe total erosion of cartilage, which was not observed in sham control rats, while AT-406-treated animals showed less severe destruction, as evidenced by reduced Safranin O staining and less surface regularity (Fig. 6A a–i). The International Association of Osteoarthritis Research (OARSI) scoring method was used to measure the changes of structural cartilage in the medial of tibial plateau and femoral condyle in all samples (Fig. 6B). The osteophyte scoring method was used to measure epiphyseal changes of the femoral condyles of all samples (Fig. 6C). We also collected photographs to evaluate the histological appearance of each group (Supplementary Fig. 5A). All samples from this experiment were independently evaluated by 2 uninformed and experienced observers. The 2 observers reached a consensus on each section.

The immunohistochemical staining for detection of IL-6 and MMP13 expression levels and activation of senescence marker genes in cartilage. As shown in Fig. 6A m-p, in ACLT-treated rats, the percentage of P16-positive chondrocytes in the PBS group was substantially higher than that in the sham surgery group, while no significant changes were observed in the low- and high-concentration AT-406 treatment groups. Similarly, the expression levels of IL-6 (Fig. 6A q–t) and MMP13 (Fig. 6A u–x) were coordinated with the expression of p16. In addition, we also tested the expression levels of c-IAP1, c-IAP2 and XIAP in cartilage. We found that the three genes of IAP family were elevated in the cartilage of OA rats (Supplementary Fig. 5B). The expression levels of p16 (Fig. 6D), IL-6 (Fig. 6E), MMP13 (Fig. 6F), c-IAP1 (Supplementary Fig. 5C), c-IAP2 (Supplementary Fig. 5D) and XIAP (Supplementary Fig. 5E) were calculated and analyzed based on the immunostaining intensity of 5 randomly selected articular cartilage regions.

2.7. AT-406 treatment attenuates tibial subchondral bone reconstruction of post-traumatic osteoarthritis in rats in vivo

Bone resorption was increased and subsequent bone hyperplasia resulted in bone reconstruction in the post-traumatic osteoarthritis (PTOA) animals. Therefore, we evaluated the therapeutic potential of AT-406 to prevent tibial subchondral bone reconstruction in vivo by ICT analysis of rat tibial subchondral bone. The 3-dimensional (3D) reconstruction results showed extensive subchondral bone hyperplasia in the ACLT group, and extensive subchondral bone reconstruction was observed compared with the sham control group, whereas intra-articular injection of AT-406 in ACLT rats significantly attenuated tibial subchondral bone reconstruction (Fig. 7A). BV/TV, BMD, SMI, Tb.N Tb.Th, and Tb.Sp were measured according to the 3D-reconstructed images (Fig. 7B).

To test the systemic potential toxicity of AT-406, the body weight of the rats was recorded twice a week during the experiment, and H&E staining was performed on the main organs including heart, liver, spleen, lung and kidney. We found no significant changes in body weight of rats injected intra-articularly with AT-406 compared with the control group (Fig. 7C). H&E staining showed that AT-406 had no obvious damage to major organs (Fig. 7D). These findings indicated that AT-406 had few toxic effects on the rats in our experiments.

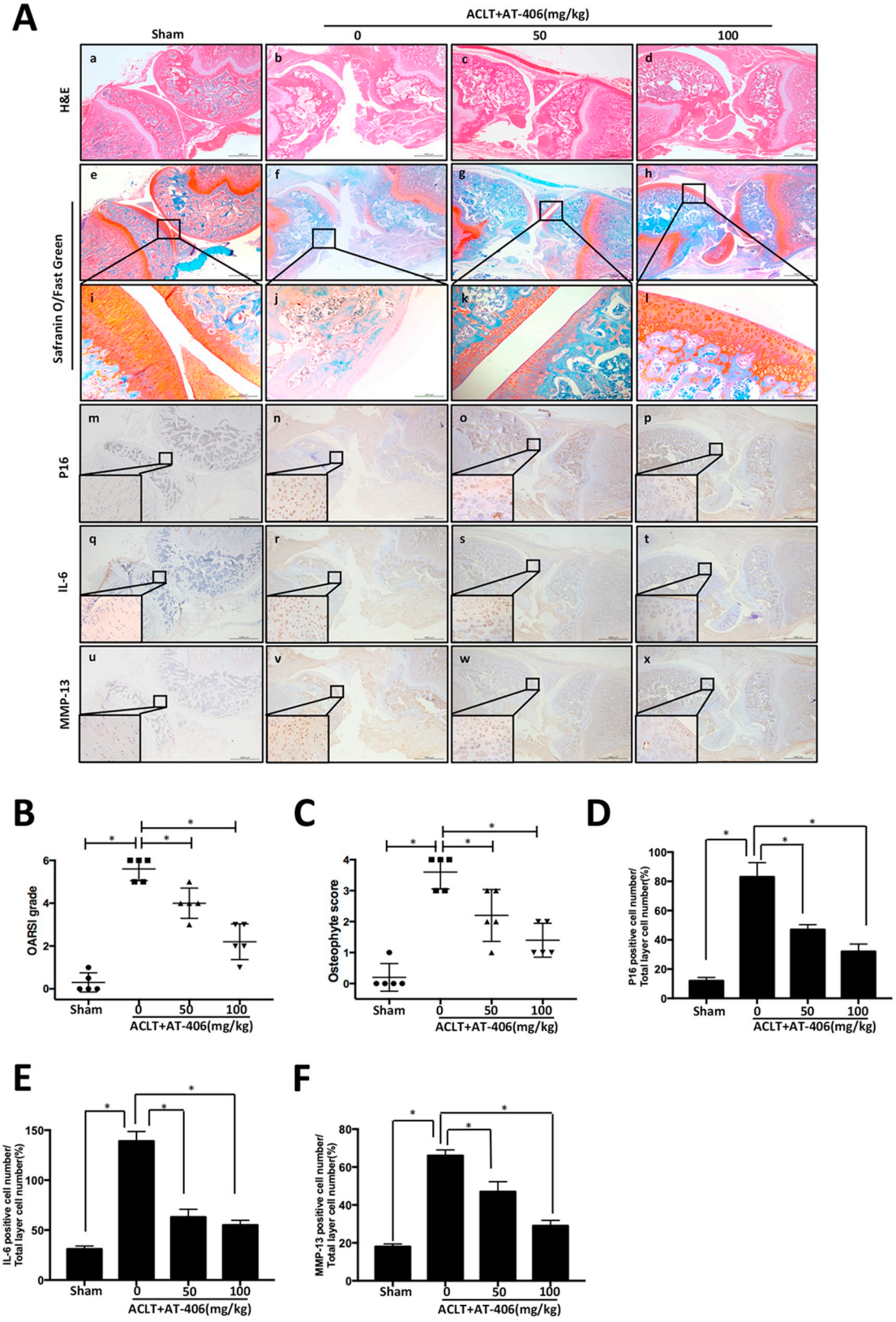

Fig. 6. Clearance of senescent cells attenuates the development of posttraumatic osteoarthritis in vivo. (A) a–l: H&E or safranin O/Fast green staining of cartilage and tibial subchondral bone. m–x: Immunohistochemical analysis of P16, IL-6 and MMP13. (B) Overall assessment of OARSI histological grade. (C) Assessment of joint surface osteophyte histological score. The immunohistochemical staining quantification of D, p16; E, IL-6; and F, MMP13. Data are shown as the mean ± SD. *P < 0.05 significantly different compared with the ACLT-operated group. The results shown here are representative of three independent experiments.

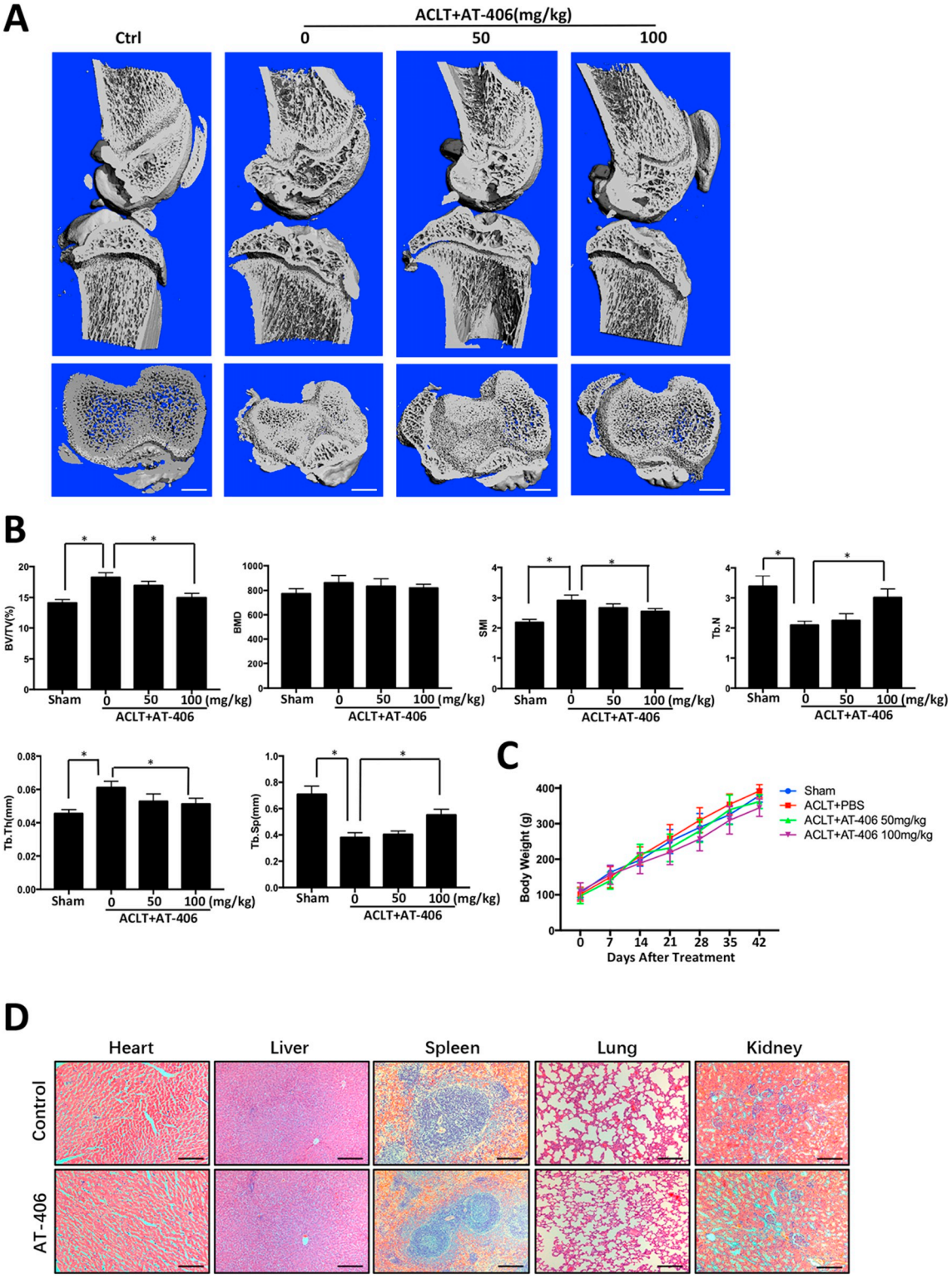

Fig. 7. Clearance of senescent cells prevents ACLT-induced bone hyperosteogeny in vivo.
(A) The microstructure of the subchondral bone was analyzed by micro-CT. Scale bar = 1 mm. (B) Statistics of bone microstructure parameters, BV/TV, BMD, Tb.Sp, Tb.Th, Tb.N and SMI. (C) The body weight was recorded twice a week. (D) H&E stained vital organs. Scale bar = 100 μm. Data are shown as the mean ± SD. *P < 0.05 significantly different compared with the ACLT-operated group. The results shown here are representative of three independent experiments.

3. Discussion

Cell senescence is a state in which cells stably arrest and proliferate and is characterized by cell cycle arrest and increased apoptosis resistance [11,26]. Our results indicate that activation of the IAP genes provides apoptosis resistance to senescent cells and supports the accumulation of senescent cells in tissues. However, such accumulation contributes to aging and promotes age-related diseases [27]. In the context of OA, aging cells were found in the vicinity of osteoarthritic lesions [28]. Consistent with this, transplanted senescent cells induced

OA-like lesions in mice [29]. Furthermore, clearing aging cells has been confirmed to delay age-related diseases in mice [30–32].

In this study, we found that resistance to apoptosis was elevated in all three types of senescent cells, consistent with the previously observed increase in apoptosis resistance in senescent cells [10,11,33]. We also found that c-IAP1, c-IAP2 and XIAP are key IAP gene family members that support the survival of senescent cells and that these proteins are upregulated by increased transcription, although the possibility of translational regulation has not been ruled out [34,35]. We found that the aging cell death rate was significantly higher when these genes were inhibited than in normal cells, and the aging cell death rate was partially restored after inhibiting the apoptosis pathway. Our data show for the first time that IAP acts as an apoptosis-inhibiting gene to provide apoptosis resistance in senescent cells. In line with previous studies that have shown that inhibition of IAP-induced apoptosis is closely related to TNF-α, we confirmed that TNF-α secretion is greatly increased in senescent cells. Therefore, inhibition of IAP-induced apoptosis in senescent cells may be associated with this [17,36,37]. Similarly, our data suggest that activation of the NF-κB pathway in senescent cells leads to an increase in IAP gene expression, which can interact with the NF-κB pathway, whereas inhibition of IAP gene expression activates the JNK pathway to promote apoptosis. This finding is consistent with previous reports, although we found that inhibition of apoptotic pathways does not completely block apoptosis caused by inhibition of IAP genes [13,21,38,39].

In the process of studying the mechanism of action of IAP, we found that inhibition of the IAP gene acts on autophagy and affects cell survival. Under normal conditions, autophagy can phagocytose and deliver cellular components to lysosomes for degradation and recycling to maintain cell homeostasis, but excessive depletion or accumulation of autophagic vacuoles can result in cell death [40,41]. Our results suggest that inhibition of IAP can block autophagosome fusion, which is consistent with previous studies. Likewise, when autophagosome synthesis is inhibited or blocked fusion is exacerbated, senescent cell death is reduced or exacerbated. In Fig. 4, we used rapamycin as a positive control, 3MA and CQ as negative controls. 3-MA and RAPA primarily target mTOR, which is an essential factor in causing autophagy. Therefore, we have detected the interaction between mTOR and IAP (Supplementary Fig. 4C). We found that inhibition of IAP reduces the activation of the mTOR pathway in normal cells and D-gal-induced senescent cells. Since inhibition of IAP can both reduce the activation of the mTOR pathway and block the fusion of autophagosomes and lysosomes, AT-406 triggers excessive autophagy of senescence and promotes the death of senescent cells. Next, we further investigated the relationship between IAP family members and autophagic lysosome fusion and found that XIAP can interact with STX17 regardless of endogenous or exogenous. Furthermore, AT-406 only inhibited the expression of XIAP, thus attenuating the interaction with STX17, but did not affect the expression of STX17. Our study demonstrates for the first time the mechanism by which XIAP affects autophagic flow. However, the relationship between apoptosis and autophagy triggered by inhibition of IAP genes remains to be resolved.

Senescent cells secrete a variety of proteins that are collectively known as the senescence-associated secretory phenotype (SASP); these proteins can induce senescence in a paracrine manner [42,43]. We found that inhibition of IAPs reduced the secretion of inflammation-related factors and restored differentiation ability, indicating that clearance of senescent cells can create a proregenerative microenvironment. OA has long been considered a disease of the cartilage but now it is acknowledged as a disease of the whole joint, including closely linked alterations in cartilage, synovium and subchondral bone [44]. In OA, the basic pathophysiological feature of OA is a loss of articular cartilage, but the degeneration of the subchondral bone precedes the articular cartilage; the subchondral bone loss occurs in the early stage of OA, and the bone resorption occurs in the subchondral bone before the cartilage degenerates [45]. MSCs are present in multiple niches in the joint, including subchondral bone, cartilage, synovial fluid, synovium and adipose tissue [46]. In previous experiments, Campbell, T. M. et al. have found that the loss of proliferative and differentiation capacity in senescent MSCs found in the bone of patients with OA [47]. Together, these studies indicate that MSCs senescence and an associated loss of potency could be an important facet of OA pathophysiology. A previous study used drugs to remove p16-positive senescent cells in gene-encoded mice to attenuate the development of PTOA [31]. However, it is still unresolved whether the goal of eliminating aging cells to delay OA can be achieved in normal animals. Next, we further investigate the potential clinical application of the clearance of senescent cell. We used ACLT to establish an OA model to evaluate the potential therapeutic effect of intra-articular AT-406 on OA cartilage destruction. We found that AT-406 rescued cartilage destruction in OA mice in a dose-dependent manner and downregulated the expression of SASP in cartilage. Thus, the clearance of senescent cells may be a new treatment for OA.

In summary, our data demonstrate for the first time that inhibition of IAP genes can eliminate senescent cells and attenuate the secretion of aging-associated inflammatory factors. This study further illustrated the effects of IAP inhibition on the expression of catabolic genes and proinflammatory cytokines during the progression of OA in vitro and the effects of AT-406 on the articular cartilage destruction caused by ACLT in vivo. We found that inhibition of IAPs activates the JNK pathway to induce apoptosis in senescent cells and that there may be interactions between the NF-κB pathway and IAPs in senescent cells, which requires further exploration. In addition, we demonstrate for the first time that XIAP interacts with STX17 to regulate the fusion of autophagy phagosomes and lysosomes. Overall, our data suggest that the clearance of senescent cells may be a new promising therapeutic strategy for OA.

4. Conclusion

Our data are the first to reveal that inhibition of the IAP genes can eliminate senescent cells and alleviate the progression of OA. We further analyzed the mechanism by which IAPs induce senescent cell death and discovered the mechanism by which XIAP regulates the fusion of autophagy phagosomes with lysosomes. We propose the removal of senescent cells as a new strategy that could be highly efficacious for the treatment of age-related diseases.

5. Materials and methods

5.1. Reagents and antibodies

The reagents used in our experiments included AT-406 (HY-15454), *Z*-VAD-FMK (HY-16658), BV6 (HY-16701), AZD5582 (HY-12600), IMD-0354 (HY-10172), CQ (HY-17589), 3MA (HY-19312) and Rapa (HY-10219), which were obtained from Medchem Express (Shanghai, China). D-gal and H_2O_2 were obtained from Shenggong (Shanghai, China) and were dissolved in dimethyl sulfoxide (DMSO) as a 10 mM stock solution for storage in aliquots at − 20 °C. Working concentrations were prepared for different experiments by diluting the stock solution with DMSO. All cell culture reagents were purchased from Invitrogen Life Technologies (Carlsbad, CA, USA). DMSO was obtained from Sigma-Aldrich (St. Louis, MO, USA). c-IAP1 (#7065), cleaved PARP (#5625), cleaved caspase-9 (#52873), cleaved caspase-3 (#9661), P21 (#2947), P53 (#9282), P65 (#8242), p-P65 (#3033), IκBα (#4814), p-IκBα (#2859), JNK (#9252), p-JNK (#9251), P38 (#8690), p-P38 (#4511), ERK (#4695), p-ERK (#4370), p-c-Jun (#9261), LC3B (#3868), SQSTM1 (#88588), BECLIN1 (#3495), MMP2 (#40994), MMP3 (#14351), MMP9 (#13667), MMP13 (#94808) and GAPDH (#5174) antibodies were purchased from Cell Signaling Technology Inc. (Danvers, MA, USA). c-IAP2 (ab23423), XIAP (ab28151), Histone H3 (ab8580), P16 (ab51243) and beta-actin (ab8224) antibodies were

purchased from Abcam (Hong Kong, China). STX17 (GTX130212) antibody was purchased from GeneTex (Shen Zhen, China).

5.2. Cell culture

Two-week-old Sprague-Dawley (SD) rats were obtained from the Experimental Animal Center of Shanghai Jiao Tong University. The laws of the People's Republic of China allow for the investigation of wildlife protection, which was approved by the Shanghai Academy of Medical Sciences in China. The femur and tibia of SD rats were removed, and the bone marrow was washed with blank medium. Cells were centrifuged at 1000 rpm for 3 min. Cells were resuspended in 5 ml Dulbecco's modified Eagle's medium/nutrition mixture F-12 (DMEM/F12, Gibco, Gaithersburg, MD, USA) supplemented with 10% fetal bovine serum (FBS, Gibco) and penicillin (100 U/ml)/streptomycin (100 U/ml) at 37 °C in humidified air with 5% CO_2 and then cultured in a 25 cm^2 plastic flask (Corning, USA) to allow the MSCs to adhere. After three days, the medium was changed, and nonadhered cells were discarded. The medium was replaced with fresh medium every 3 days. After approximately 7–10 days, adherent cells were released from the flask with 0.25% trypsin (Gibco) and inoculated into new flasks. These cells were labeled passage 1, and the cells were cultured until passage 3. All cells experiments except those for the RS group of cells were performed using passage 3 cells; and experiments for the RS group of cells were performed using passage 7 cells.

5.3. Cell viability assay

Cell proliferation was measured by a CCK-8 assay (Dojindo, Tokyo, Japan). The cell suspension (4×10^4/ml) was inoculated into 96-well plates overnight and then treated with various concentrations of experimental reagent. If the experimental reagent was dissolved in DMSO, the concentration of DMSO was maintained at $< 0.5\%$ in all wells. After 24, 48 and 72 h, each well was incubated with 90 μl of fresh medium and 10 μl of CCK-8 solution for 2 h at 37 °C, and then, the absorbance was read at a wavelength of 450 nm.

5.4. Cell cycle analysis by flow cytometry

Cells were seeded at a density of 5×10^5/ml in a six-well plate and treated with D-gal (10 g/l) or H_2O_2 (100 μM) for 48 h and passaged to the seventh passage. Then, the cells were harvested and fixed overnight at 4 °C with cold 70% ethanol. The cells were again washed with PBS, incubated with RNase A for 30 min, and then stained with 400 μl propidium iodide (PI) for 30 min at room temperature. Cell cycle analysis was performed on an Accuri C6 flow cytometer (BD Biosciences, Mountain View, CA, USA).

5.5. Apoptosis analysis by flow cytometry

The effect of AT-406 on apoptosis was analyzed by flow cytometry using Annexin V-FITC and PI. Cells were seeded at a density of 5×10^5/ml in a six-well plate, and cell senescence was induced by different methods, followed by treatment with AT-406 (10 μM) for 48 h. z-VAD-fmk was added to the cell culture at a concentration of 100 mM 4 h before AT-406 addition. Then, the cells were harvested, washed twice with cold PBS, and resuspended in 1× binding buffer. The cells were incubated with Annexin V-FITC and PI at room temperature in the dark for 15 min using an Accuri C6 flow cytometer (BD Biosciences, Mountain View, CA, USA).

5.6. SA-β-gal staining

The expression of senescence-associated b-galactosidase (SA-β-gal) in BMSCs has been used as a typical biomarker for premature aging. SA-β-gal staining was performed using a SA-β-gal staining kit (Cell Signaling Technology, Beverly, MA, USA) according to the manufacturer's instructions. Cells were incubated overnight at 37 °C in the absence of CO_2. The number of positive cells was counted using a phase contrast microscope, and the experiment was repeated five times for each group.

5.7. Western blotting and coimmunoprecipitation

Cells were lysed with ice-cold radioimmunoprecipitation (RIPA) buffer containing a protease inhibitor cocktail (Sigma-Aldrich) for 30 min. The soluble protein lysate concentration was then determined using a bicinchoninic acid (BCA) Protein Assay Kit (Thermo Scientific, Fremont, CA, USA). Proteins were separated by 10–12% SDS-PAGE and transferred onto polyvinylidene difluoride (PVDF) membranes. Membranes were incubated in 5% nonfat milk in PBST buffer for 1 h at room temperature and incubated overnight at 4 °C on a shaker with specific primary antibodies. The membranes were washed with TBST and then incubated with secondary antibody (Sigma-Aldrich, Inc.) for 1 h at room temperature. After washing three times, signal bands were detected using an enhanced chemiluminescence kit (Millipore). For coimmunoprecipitation assays, whole cell lysates of samples treated with or without D-gal and AT-406 were incubated overnight with specific antibodies for precipitation, and then with protein A/G-agarose beads were incubated together. Finally, the samples were washed five times with washing buffer. The eluted proteins were separated by 10% SDS-PAGE. Independent experiments were performed in triplicate.

Flag M2 Affinity Gel (Sigma, A2220) was used to immunoprecipitate the Flag-tagged proteins. After three washes with clod 1× TBS, the immunoprecipitated protein complexes were eluted through 3× Flag peptides (Sigma, F4799). The coimmunoprecipitated proteins were detected by Western blot analysis.

5.8. RNA extraction and quantitative real-time PCR analysis

According to the manufacturer's protocol, RNA samples were prepared from cells using Trizol reagent (Invitrogen, Carlsbad, CA, USA). Total RNA (1 μg) was converted to cDNA using a Reverse Transcription Kit (TaKaRa Inc., RR036A, JAPAN). The relative expression of glutathione reductase (GR) was analyzed by qPCR, and actin was used as an internal control. The primer sequences can be found in Supplementary Table 1.

5.9. Immunofluorescence

Cultured cells in glass-bottom dishes were fixed with 4% paraformaldehyde (PFA) for 30 min with blocking buffer (containing 10% goat serum and 1% bovine serum albumin (BSA) in PBS) and incubated at room temperature for 1 h. P65 antibody (1:400 dilution), c-IAP1 antibody (1:400 dilution), c-IAP2 antibody (1:400 dilution) in PBS and XIAP antibody (1:400 dilution) were added, and cells were incubated overnight at 4 °C. Cells were then washed 3 times with TBST solution for 5 min each time and then incubated with Alexa Fluor 594 (Life Technologies, USA)-conjugated goat anti-rabbit IgG antibody diluted 1:200 in PBS in the dark at room temperature for 30 min. Cells were washed 3 times with TBST solution for 5 min each time, and nuclear DNA was then stained with DAPI (Dojindo, Japan) for 3 min. After washing 3 times for 5 min each time, the culture dish was covered with PBS, and an image was acquired using a fluorescence confocal microscope (Olympus, Japan).

5.10. ELISA

MMPs and inflammatory cytokines, especially IL-1β, IL-6 and TNF-α, are thought to mediate the progression of OA. Superfilts from different groups of BMSCs were collected and analyzed using an ELISA kit (R&D Systems, Minneapolis, MN, USA) according to the manufacturer's

instructions. The results are expressed in picograms per milligram.

5.11. Nuclear and cytoplasmic extraction

BMSCs were treated with D-gal for 48 h. To isolate cytoplasmic and nuclear proteins, cell pellets were treated using a nuclear and cytoplasmic extraction kit (Beyotime, NanJing, China) according to the manufacturer's instructions.

5.12. Osteogenic differentiation

The BMSCs-encapsulating gelatin were maintained in 2 mL osteoinductive medium containing 0.05 mM L-ascorbic acid, 10 mM β-sodium glycerol phosphate, and 100 nM dexamethasone sodium phosphate. Add the corresponding conditioned medium as a control group, aging group and aging treatment group. The medium was replaced every 2 days. After 3 weeks of culture, the cells were fixed for 10 min in formalin and stained with alizarin red.

5.13. Chondrogenic differentiation

BMSCs (2.5×10^5) were induced to form a chondrogenic pellet using chondrogenic differentiation medium according to the manufacturer's description. Add the corresponding conditioned medium as a control group, aging group and aging treatment group. Culture media were changed every two days. After 4 weeks of culture, the pellets were harvested for histological assessment.

5.14. ACLT-mediated knee OA and treatment

All animal procedures were performed in accordance with a protocol approved by the Animal Care and Use Committee of Shanghai General Hospital and Shanghai Jiaotong University. Twenty male Sprague-Dawley rats (4 weeks old) were divided into a sham operation group and an ACLT group. After anesthesia, a medial para-abdominal articular incision was made on the right knee of the animal using a sterile surgical instrument. The medial collateral ligament and anterior cruciate ligament were dissected, and the medial meniscus was removed. The sham operation group did the cut-off capsule but not the ACLT. The joint capsule and skin were then sutured with absorbable threads. Postoperative pain medication of 0.02 mg/kg fentanyl citrate (fentanyl; Abbott, Chicago, Illinois) was administered subcutaneously twice daily for 3 days after the operation. Rats were randomly divided into the following four groups: Group I (sham operation group, $n = 5$) rats were not operated or treated; Group II (ACLT + vector, n = 5) rats were subjected to ACLT and intra-articularly injected with PBS (10 μl, three times a week); Group III (ACLT + low dose AT-406, n = 5) rats received ACLT and intra-articular injection of low dose AT-406 (50 mg/kg, 10 μl, three times a week); Group IV (ACLT + high dose AT-406, n = 5) rats underwent ACLT surgery and intra-articular injection of AT-406 (100 mg/kg, 10 μl, three times a week). Rats were housed under a 12 h light/dark cycle at a constant temperature of 24 ± 2 °C and a relative humidity of 55% ± 5% and allowed free access to food and water. Rats were allowed to move freely in the cage after surgery.

5.15. Histological assessments

All animals were sacrificed 6 weeks after surgery. Knee samples were collected and fixed in 4% paraformaldehyde for 24 h. After decalcification in 10% EDTA for several days, the samples were embedded in paraffin, cut into 4-μm sections, and stained with hematoxylin and eosin (H&E) or Safranin O/fast green staining, as described above for further histological analysis. Semiquantitative scoring of histopathological features was performed according to the OARSI rating system, which includes 6 histological grades and 4 histological stages. The total score (score = grade × stage) ranged from 1 point (normal articular cartilage) to 24 points (no repair). Each of the three independent observers scored each score and averaged the scores for all of the sections in each sample. All scores were performed by three independent observers blinded to the treatment group. All procedures considered animal welfare and were reviewed and approved by the Shanghai General Hospital Ethics Committee.

5.16. Immunohistochemical analysis

The sections were dewaxed with xylene and rehydrated in a graded series of ethanol. The sections were blocked with 3% H_2O_2 to reduce endogenous peroxide and then prepared by enzymatic digestion with proteinase K (10 mM, Sigma, St. Louis, MO, USA) in PBS. Tablets were used for antigen retrieval. After 15 min of blocking with 1% BSA for 15 min to inhibit nonspecific staining, sections were paired with cleaved caspase-3 (dilution 1:200), P16 (dilution 1:50), P21 (dilution 1:50), IL-6 (dilution 1:400), MMP9 (dilution 1:400), c-IAP1 (dilution 1:100), c-IAP2 (dilution 1:100) and XIAP (dilution 1: 400). Sections were incubated with the primary antibody overnight at 4 °C and then incubated with the biotinylated secondary antibody. The reaction was developed using a DAB kit (BD Bioscience, Franklin Lakes, NJ, USA), and the tissue was counterstained with hematoxylin. Blind assessment of immunoreactivity was performed independently by two pathologists. The proportion of immunopositive cells was assessed.

5.17. Micro-CT analysis

After treatment, all hind limbs of the mice were dissected and fixed in 4% PFA for 24 h, followed by micro-CT analysis. Axial scanning was performed using high resolution lCT (70 kv, 200 μA) by YUEBO Corporation (Hangzhou, China). The sagittal sections were then reconstructed at a resolution of 10 lm. The subchondral bone under the tibial plateau region was defined as the region of interest (ROI). Analysis of trabecular bone, including bone mineral density (BMD), bone volume/total tissue volume (BV/TV), trabecular number (Tb.N), trabecular thickness (Tb.Th), trabecular separation (Tb.Sp) and structural model index (SMI), were performed using software provided by the manufacturer.

5.18. Statistical analysis

Data are expressed as the mean ± SD. Student's *t*-test was used to determine statistical significance. The criterion for statistical significance was considered to be $P < 0.05$.

Supplementary data to this article can be found online at https://doi.org/10.1016/j.bbadis.2019.05.017.

Abbreviations

SnCs	senescence cells
SASP	senescence-associated secretory phenotype
OA	osteoarthritis
BMSC	bone marrow mesenchymal stem cells
IAP	inhibitor of apoptosis protein
DS	D-gal induces senescence
HS	H_2O_2 induces senescence
RS	replicative senescence
CHX	cycloheximide
PARP	poly-ADP-ribose polymerase
NF-κB	nuclear factor kappaB
IκBα	IkappaBalpha
MAPK	mitogen-activated protein kinase
JNK	c-Jun N-terminal kinase
ERK	extracellular regulated protein kinases
CQ	chloroquine
3MA	3-methyladenine

Rapa	rapamycin
ACLT	anterior cruciate ligament transection
DMSO	dimethyl sulfoxide
FBS	fetal bovine serum

Declarations

Ethics approval and consent to participate

Use of nude mice was approved by the Animal Care and Use Committee of Shanghai General Hospital and Shanghai Jiaotong University. (Shanghai, China).

Transparency document

The Transparency document associated with this article can be found, in online version.

Acknowledgements

This work was supported by the NSFC (NO. 81371979, NO. 81702114, NO. 81501584) and Shanghai Pujiang Program (17PJ1408100). The authors thank the Institute of Central Laboratory of Shanghai General Hospital for providing parts of the experimental apparatus. We also thank Mr. Lang Tao and Mr. Tang Jinhua (Shanghai General Hospital, Shanghai Jiao Tong University School of Medicine) for their assistance.

Conflict of interests

All authors declare that they have no conflicts of interest concerning this article.

References

[1] M.J. Regulski, Cellular senescence: what, why, and how, Wounds : A Compendium of Clinical Research and Practice 29 (6) (2017) 168–174.
[2] B.G. Childs, M. Gluscevic, D.J. Baker, R.M. Laberge, D. Marquess, J. Dananberg, J.M. van Deursen, Senescent cells: an emerging target for diseases of ageing, Nat. Rev. Drug Discov. 16 (10) (2017) 718–735, https://doi.org/10.1038/nrd.2017.116.
[3] T. Tchkonia, Y. Zhu, J. van Deursen, J. Campisi, J.L. Kirkland, Cellular senescence and the senescent secretory phenotype: therapeutic opportunities, J. Clin. Invest. 123 (3) (2013) 966–972, https://doi.org/10.1172/jci64098.
[4] K. McCulloch, G.J. Litherland, T.S. Rai, Cellular senescence in osteoarthritis pathology, Aging Cell 16 (2) (2017) 210–218, https://doi.org/10.1111/acel.12562.
[5] R.F. Loeser, J.A. Collins, B.O. Diekman, Ageing and the pathogenesis of osteoarthritis, Nat. Rev. Rheumatol. 12 (7) (2016) 412–420, https://doi.org/10.1038/nrrheum.2016.65.
[6] J. Oh, Y.D. Lee, A.J. Wagers, Stem cell aging: mechanisms, regulators and therapeutic opportunities, Nat. Med. 20 (8) (2014) 870–880, https://doi.org/10.1038/nm.3651.
[7] M. Xu, T. Pirtskhalava, J.N. Farr, B.M. Weigand, A.K. Palmer, M.M. Weivoda, C.L. Inman, M.B. Ogrodnik, C.M. Hachfeld, D.G. Fraser, J.L. Onken, K.O. Johnson, G.C. Verzosa, L.G.P. Langhi, M. Weigl, N. Giorgadze, N.K. LeBrasseur, J.D. Miller, D. Jurk, R.J. Singh, D.B. Allison, K. Ejima, G.B. Hubbard, Y. Ikeno, H. Cubro, V.D. Garovic, X. Hou, S.J. Weroha, P.D. Robbins, L.J. Niedernhofer, S. Khosla, T. Tchkonia, J.L. Kirkland, Senolytics improve physical function and increase lifespan in old age, Nat. Med. 24 (8) (2018) 1246–1256, https://doi.org/10.1038/s41591-018-0092-9.
[8] J.N. Farr, M. Xu, M.M. Weivoda, D.G. Monroe, D.G. Fraser, J.L. Onken, B.A. Negley, J.G. Sfeir, M.B. Ogrodnik, C.M. Hachfeld, N.K. LeBrasseur, M.T. Drake, R.J. Pignolo, T. Pirtskhalava, T. Tchkonia, M.J. Oursler, J.L. Kirkland, S. Khosla, Targeting cellular senescence prevents age-related bone loss in mice, Nat. Med. 23 (9) (2017) 1072–1079, https://doi.org/10.1038/nm.4385.
[9] M. Ogrodnik, H. Salmonowicz, V.N. Gladyshev, Integrating cellular senescence with the concept of damage accumulation in aging: relevance for clearance of senescent cells, Aging Cell (2018) e12841, , https://doi.org/10.1111/acel.12841.
[10] R. Yosef, N. Pilpel, R. Tokarsky-Amiel, A. Biran, Y. Ovadya, S. Cohen, E. Vadai, L. Dassa, E. Shahar, R. Condiotti, I. Ben-Porath, V. Krizhanovsky, Directed elimination of senescent cells by inhibition of BCL-W and BCL-XL, Nat. Commun. 7 (2016) 11190, , https://doi.org/10.1038/ncomms11190.
[11] A. Salminen, J. Ojala, K. Kaarniranta, Apoptosis and aging: increased resistance to apoptosis enhances the aging process. Cellular and molecular life sciences, CMLS 68 (6) (2011) 1021–1031, https://doi.org/10.1007/s00018-010-0597-y.
[12] J. Silke, P. Meier, Inhibitor of apoptosis (IAP) proteins-modulators of cell death and inflammation, Cold Spring Harb. Perspect. Biol. 5 (2) (2013), https://doi.org/10.1101/cshperspect.a008730.
[13] M. Gyrd-Hansen, P. Meier, IAPs: from caspase inhibitors to modulators of NF-kappaB, inflammation and cancer, Nat. Rev. Cancer 10 (8) (2010) 561–574, https://doi.org/10.1038/nrc2889.
[14] L. Dubrez-Daloz, A. Dupoux, J. Cartier, IAPs: more than just inhibitors of apoptosis proteins, Cell Cycle (Georgetown, Tex) 7 (8) (2008) 1036–1046, https://doi.org/10.4161/cc.7.8.5783.
[15] F.G. Osorio, C. Soria-Valles, O. Santiago-Fernandez, J.M. Freije, C. Lopez-Otin, NF-kappaB signaling as a driver of ageing, Int. Rev. Cell Mol. Biol. 326 (2016) 133–174, https://doi.org/10.1016/bs.ircmb.2016.04.003.
[16] J. Silke, D. Vucic, IAP family of cell death and signaling regulators, Methods Enzymol. 545 (2014) 35–65, https://doi.org/10.1016/b978-0-12-801430-1.00002-0.
[17] E. Varfolomeev, J.W. Blankenship, S.M. Wayson, A.V. Fedorova, N. Kayagaki, P. Garg, K. Zobel, J.N. Dynek, L.O. Elliott, H.J. Wallweber, J.A. Flygare, W.J. Fairbrother, K. Deshayes, V.M. Dixit, D. Vucic, IAP antagonists induce autoubiquitination of c-IAPs, NF-kappaB activation, and TNFalpha-dependent apoptosis, Cell 131 (4) (2007) 669–681, https://doi.org/10.1016/j.cell.2007.10.030.
[18] E. Varfolomeev, D. Vucic, (Un)expected roles of c-IAPs in apoptotic and NFkappaB signaling pathways, Cell Cycle (Georgetown, Tex) 7 (11) (2008) 1511–1521, https://doi.org/10.4161/cc.7.11.5959.
[19] S. Galban, C.S. Duckett, XIAP as a ubiquitin ligase in cellular signaling, Cell Death Differ. 17 (1) (2010) 54–60, https://doi.org/10.1038/cdd.2009.81.
[20] S. Gardam, V.M. Turner, H. Anderton, S. Limaye, A. Basten, F. Koentgen, D.L. Vaux, J. Silke, R. Brink, Deletion of cIAP1 and cIAP2 in murine B lymphocytes constitutively activates cell survival pathways and inactivates the germinal center response, Blood 117 (15) (2011) 4041–4051, https://doi.org/10.1182/blood-2010-10-312793.
[21] S. Papa, C. Bubici, F. Zazzeroni, C.G. Pham, C. Kuntzen, J.R. Knabb, K. Dean, G. Franzoso, The NF-kappaB-mediated control of the JNK cascade in the antagonism of programmed cell death in health and disease, Cell Death Differ. 13 (5) (2006) 712–729, https://doi.org/10.1038/sj.cdd.4401865.
[22] P. Ebner, I. Poetsch, L. Deszcz, T. Hoffmann, J. Zuber, F. Ikeda, The IAP family member BRUCE regulates autophagosome-lysosome fusion, Nat. Commun. 9 (1) (2018) 599, https://doi.org/10.1038/s41467-018-02823-x.
[23] S. Gradzka, O.S. Thomas, O. Kretz, A. Haimovici, L. Vasilikos, W.W. Wong, G. Hacker, I.E. Gentle, Inhibitor of apoptosis proteins are required for effective fusion of autophagosomes with lysosomes, Cell Death Dis. 9 (5) (2018) 529, https://doi.org/10.1038/s41419-018-0508-y.
[24] X. Li, F. Zhu, J. Jiang, C. Sun, Q. Zhong, M. Shen, X. Wang, R. Tian, C. Shi, M. Xu, F. Peng, X. Guo, J. Hu, D. Ye, M. Wang, R. Qin, Simultaneous inhibition of the ubiquitin-proteasome system and autophagy enhances apoptosis induced by ER stress aggravators in human pancreatic cancer cells, Autophagy 12 (9) (2016) 1521–1537, https://doi.org/10.1080/15548627.2016.1191722.
[25] T. Kimura, J. Jia, A. Claude-Taupin, S. Kumar, S.W. Choi, Y. Gu, M. Mudd, N. Dupont, S. Jiang, R. Peters, F. Farzam, A. Jain, K.A. Lidke, C.M. Adams, T. Johansen, V. Deretic, Cellular and molecular mechanism for secretory autophagy, Autophagy 13 (6) (2017) 1084–1085, https://doi.org/10.1080/15548627.2017.1307486.
[26] B.G. Childs, D.J. Baker, J.L. Kirkland, J. Campisi, J.M. van Deursen, Senescence and apoptosis: dueling or complementary cell fates? EMBO Rep. 15 (11) (2014) 1139–1153, https://doi.org/10.15252/embr.201439245.
[27] B.G. Childs, M. Durik, D.J. Baker, J.M. van Deursen, Cellular senescence in aging and age-related disease: from mechanisms to therapy, Nat. Med. 21 (12) (2015) 1424–1435, https://doi.org/10.1038/nm.4000.
[28] A. Hou, P. Chen, H. Tang, H. Meng, X. Cheng, Y. Wang, Y. Zhang, J. Peng, Cellular senescence in osteoarthritis and anti-aging strategies, Mech. Ageing Dev. 175 (2018) 83–87, https://doi.org/10.1016/j.mad.2018.08.002.
[29] M. Xu, E.W. Bradley, M.M. Weivoda, S.M. Hwang, T. Pirtskhalava, T. Decklever, G.L. Curran, M. Ogrodnik, D. Jurk, K.O. Johnson, V. Lowe, T. Tchkonia, J.J. Westendorf, J.L. Kirkland, Transplanted senescent cells induce an osteoarthritis-like condition in mice, The journals of gerontology Series A, Biological Sciences and Medical Sciences 72 (6) (2017) 780–785, https://doi.org/10.1093/gerona/glw154.
[30] D.J. Baker, T. Wijshake, T. Tchkonia, N.K. LeBrasseur, B.G. Childs, B. van de Sluis, J.L. Kirkland, J.M. van Deursen, Clearance of p16Ink4a-positive senescent cells delays ageing-associated disorders, Nature 479 (7372) (2011) 232–236, https://doi.org/10.1038/nature10600.
[31] O.H. Jeon, C. Kim, R.M. Laberge, M. Demaria, S. Rathod, A.P. Vasserot, J.W. Chung, D.H. Kim, Y. Poon, N. David, D.J. Baker, J.M. van Deursen, J. Campisi, J.H. Elisseeff, Local clearance of senescent cells attenuates the development of post-traumatic osteoarthritis and creates a pro-regenerative environment, Nat. Med. 23 (6) (2017) 775–781, https://doi.org/10.1038/nm.4324.
[32] T.J. Bussian, A. Aziz, C.F. Meyer, B.L. Swenson, J.M. van Deursen, D.J. Baker, Clearance of senescent glial cells prevents tau-dependent pathology and cognitive decline, Nature 562 (7728) (2018) 578–582, https://doi.org/10.1038/s41586-018-0543-y.
[33] J. Tower, Programmed cell death in aging, Ageing Res. Rev. 23 (Pt A) (2015) 90–100, https://doi.org/10.1016/j.arr.2015.04.002.
[34] D. Vasudevan, H.D. Ryoo, Regulation of cell death by IAPs and their antagonists, Curr. Top. Dev. Biol. 114 (2015) 185–208, https://doi.org/10.1016/bs.ctdb.2015.07.026.
[35] J. Silke, J. Vince, IAPs and cell death, Curr. Top. Microbiol. Immunol. 403 (2017) 95–117, https://doi.org/10.1007/82_2016_507.
[36] J.E. Vince, W.W. Wong, N. Khan, R. Feltham, D. Chau, A.U. Ahmed, C.A. Benetatos, S.K. Chunduru, S.M. Condon, M. McKinlay, R. Brink, M. Leverkus, V. Tergaonkar,

P. Schneider, B.A. Callus, F. Koentgen, D.L. Vaux, J. Silke, IAP antagonists target cIAP1 to induce TNFalpha-dependent apoptosis, Cell 131 (4) (2007) 682–693, https://doi.org/10.1016/j.cell.2007.10.037.

[37] M. Saleem, M.I. Qadir, N. Perveen, B. Ahmad, U. Saleem, T. Irshad, B. Ahmad, Inhibitors of apoptotic proteins: new targets for anticancer therapy, Chem. Biol. Drug Des. 82 (3) (2013) 243–251, https://doi.org/10.1111/cbdd.12176.

[38] S. Papa, F. Zazzeroni, C.G. Pham, C. Bubici, G. Franzoso, Linking JNK signaling to NF-kappaB: a key to survival, J. Cell Sci. 117 (2004) 5197–5208, https://doi.org/10.1242/jcs.01483 Pt 22.

[39] G. Tang, Y. Minemoto, B. Dibling, N.H. Purcell, Z. Li, M. Karin, A. Lin, Inhibition of JNK activation through NF-kappaB target genes, Nature 414 (6861) (2001) 313–317, https://doi.org/10.1038/35104568.

[40] L. Galluzzi, E.H. Baehrecke, A. Ballabio, P. Boya, J.M. Bravo-San Pedro, F. Cecconi, A.M. Choi, C.T. Chu, P. Codogno, M.I. Colombo, A.M. Cuervo, J. Debnath, V. Deretic, I. Dikic, E.L. Eskelinen, G.M. Fimia, S. Fulda, D.A. Gewirtz, D.R. Green, M. Hansen, J.W. Harper, M. Jaattela, T. Johansen, G. Juhasz, A.C. Kimmelman, C. Kraft, N.T. Ktistakis, S. Kumar, B. Levine, C. Lopez-Otin, F. Madeo, S. Martens, J. Martinez, A. Melendez, N. Mizushima, C. Munz, L.O. Murphy, J.M. Penninger, M. Piacentini, F. Reggiori, D.C. Rubinsztein, K.M. Ryan, L. Santambrogio, L. Scorrano, A.K. Simon, H.U. Simon, A. Simonsen, N. Tavernarakis, S.A. Tooze, T. Yoshimori, J. Yuan, Z. Yue, Q. Zhong, G. Kroemer, Molecular definitions of autophagy and related processes, EMBO J. 36 (13) (2017) 1811–1836, https://doi.org/10.15252/embj.201796697.

[41] K. Hegedus, S. Takats, A.L. Kovacs, G. Juhasz, Evolutionarily conserved role and physiological relevance of a STX17/Syx17 (syntaxin 17)-containing SNARE complex in autophagosome fusion with endosomes and lysosomes, Autophagy 9 (10) (2013) 1642–1646, https://doi.org/10.4161/auto.25684.

[42] S. He, N.E. Sharpless, Senescence in health and disease, Cell 169 (6) (2017) 1000–1011, https://doi.org/10.1016/j.cell.2017.05.015.

[43] R. Salama, M. Sadaie, M. Hoare, M. Narita, Cellular senescence and its effector programs, Genes Dev. 28 (2) (2014) 99–114, https://doi.org/10.1101/gad.235184.113.

[44] D.C. Ilas, S.M. Churchman, D. McGonagle, E. Jones, Targeting subchondral bone mesenchymal stem cell activities for intrinsic joint repair in osteoarthritis, Future Science OA 3 (4) (2017) Fso228, https://doi.org/10.4155/fsoa-2017-0055.

[45] H.L. Stewart, C.E. Kawcak, The importance of subchondral bone in the pathophysiology of osteoarthritis, Frontiers in Veterinary Science 5 (2018) 178, , https://doi.org/10.3389/fvets.2018.00178.

[46] D. McGonagle, T.G. Baboolal, E. Jones, Native joint-resident mesenchymal stem cells for cartilage repair in osteoarthritis, Nat. Rev. Rheumatol. 13 (12) (2017) 719–730, https://doi.org/10.1038/nrrheum.2017.182.

[47] T.M. Campbell, S.M. Churchman, A. Gomez, D. McGonagle, P.G. Conaghan, F. Ponchel, E. Jones, Mesenchymal stem cell alterations in bone marrow lesions in patients with hip osteoarthritis, Arthritis & Rheumatology (Hoboken, NJ) 68 (7) (2016) 1648–1659, https://doi.org/10.1002/art.39622.